CORROSION SCIENCE AND TECHNOLOGY, Vol.11, No.1(2012), pp.1~8

Development of Continuous Galvanization-compatible Martensitic Steel

Y. F. Gong[1], T. J. Song[1], Han S. Kim[1], J. H. Kwak[2], and B. C. De Cooman[1,†]

[1]*Materials Design Laboratory, Graduate Institute of Ferrous Technology, Pohang University of Science and Technology, Pohang, South Korea*
[2]*Automotive Steel Research Group, POSCO Gwangyang Works, Gwangyang, South Korea*
(Received August 3, 2009; No Revision; Accepted February 24, 2012)

The development of martensitic grades which can be processed in continuous galvanizing lines requires the reduction of the oxides formed on the steel during the hot dip process. This reduction mechanism was investigated in detail by means of High Resolution Transmission Electron Microscopy (HR-TEM) of cross-sectional samples. Annealing of a martensitic steel in a 10% H_2 + N_2 atmosphere with the dew point of -35 ℃ resulted in the formation of a thin *c*-x$MnO.SiO_2$ (x>1) oxide film and amorphous *a*-x$MnO.SiO_2$ oxide particles on the surface. During the hot dip galvanizing in Zn-0.13%Al, the thin *c*-x$MnO.SiO_2$ (x>1) oxide film was reduced by the Al. The *a*-x$MnO.SiO_2$ (x<0.9) and *a*-SiO_2 oxides however remained embedded in the Zn coating close to the steel/coating interface. No $Fe_2Al_{5-x}Zn_x$ inhibition layer formation was observed. During hot dip galvanizing in Zn-0.20%Al, the *c*-x$MnO.SiO_2$ (x>1) oxide film was also reduced and the amorphous *a*-x$MnO.SiO_2$ and *a*-SiO_2 particles were embedded in the $Fe_2Al_{5-x}Zn_x$ inhibition layer formed at the steel/coating interface during hot dipping. The results clearly show that Al in the liquid Zn bath can reduce the crystalline *c*-x$Mn.SiO_2$ (x>1) oxides but not the amorphous *a*-x$MnO.SiO_2$ (x<0.9) and *a*-SiO_2 oxides. These oxides remain embedded in the Zn layer or in the inhibition layer, making it possible to apply a Zn or Zn-alloy coating on martensitic steel by hot dipping. The hot dipping process was also found to deteriorate the mechanical properties, independently of the Zn bath composition.

Keywords *: martensitic steel, hot dip galvanizing, oxides, HR-TEM*

1. Introduction

Current automotive body-in-white designs place a great emphasis on passenger safety aspects. Whereas DP and TRIP steels are ideally suited for energy absorption in frontal collision, martensitic grades must be used for anti-intrusion barriers to protect passengers in case of side collision or roll over. Furthermore, the corrosion resistance must be ensured for any material used in a structural part of automotive components. In this regard, continuous hot-dip galvanization-compatible martensitic steel is a very promising material, which can provide ultra-high strength and a cost-effective approach to perforation corrosion resistance. Conventional hot-dip coating processes, however, can result in micro-structural changes of the matrix phase leading to loss of strength. Therefore, optimal addition of alloying elements is crucial in designing the material for improved hardenability and for stabilizing the desired microstructure. However, at the same time, the alloy system must have a lean chemical composition so as not to cause coating defects during the hot-dip coating process and ensure good weldability. The present contribution mainly focuses on (1) the selective oxidation reactions at the surface and in the sub-surface of martensitic steel during austenitic annealing, (2) the effect of the Zn bath composition on the oxides present on the martensitic steel prior to hot dipping, and (3) the effect of the hot dipping coating process on the mechanical properties of martensitic steel.

The gas atmosphere of the industrial annealing furnace in continuous hot dip Galvanizing/Galvannealing (GI/GA) lines leads to the reduction of the iron oxides formed during cold rolling and the selective oxidation of the key alloying additions of Mn, Al and Si. The presence of film-forming surface oxides at the steel surface prior to hot dipping has been reported as having a significant effect on the wettability of the steel by molten Zn and their presence may prevent the formation of the $Fe_2Al_{5-x}Zn_x$ inhibition layer.[1)-5)] The formation of surface oxides during

† Corresponding author: decooman@postech.ac.kr

the annealing of Si-bearing steels is very well documented.[2),6)-10)] There are very few direct observations of the formation of the oxides during the annealing, the interaction of the oxides with the Zn bath and the effect of the oxides on the wetting of the steel surface by the liquid Zn. Khondker *et al*. and Bellhouse *et al*. have reported that oxides formed on the surface of TRIP and DP steel can be reduced by the Al during the dipping process.[11),12)] Meguerian *et al*. reported the reactive wetting kinetics of MnO on Mn-bearing DP steel surface.[13)] The direct observation of the interaction between actual surface oxides present on Advanced High Strength Steel (AHSS), i.e. *a*-SiO_2, *a*-x$MnO.SiO_2$, *c*-$MnO.SiO_2$ and *c*-$2MnO.SiO_2$, and the Al in the Zn bath has not yet been reported.

In the present study, the morphology, size, distribution and composition of the oxides formed on low-Si martensitic steel prior to galvanizing were directly observed by High-Resolution Transmission Electron Microscopy (HR-TEM) of Focused Ion Beam (FIB) cross-sectional samples, and the interactions between the oxides and the Zn bath were investigated.

2. Experimental

The martensitic steel used in the present work was a full-hard cold-rolled steel with a thickness of 1 mm containing 0.15 mass% C, 2.0 mass% Mn and 0.33 mass% Si. The sample surface was degreased in a 2% NaOH solution and ultrasonically cleaned in iso-propanol prior to the annealing simulation. The hot dip galvanizing (HDG) process simulation was carried out in a HDG simulator. The 10%H_2+N_2 gas atmosphere had a dew point of -35 ℃. The Zn bath compositions were 0.13% Al and 0.20% Al for the simulation of the interactions between steel and the liquid Zn in conditions comparable to galvannealing and galvanizing, respectively.

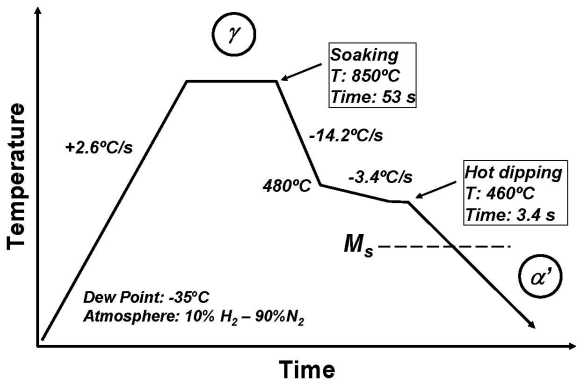

Fig. 1. Schematic of the thermal cycle used for the GI/GA experiments. The 10%H_2 + 90%N_2 gas atmosphere had a dew point of -35 ℃.

The thermal cycle is shown in Fig. 1. The annealing temperature (850 ℃) was in the fully austenitic phase stability range. The soaking time was 53 seconds. The temperature of the Zn bath was 460 ℃ and the dip time was 3.4 seconds. Coated and uncoated samples were analyzed in a 200 keV JEOL JEM-2100F using FIB cross-sectional samples. Tensile specimens were machined from the coated steel panels and tensile tests were performed at room temperature on a Zwick/Roell universal testing machine using a strain rate of 10^{-3}/s.

3. Results and discussion

A typical cross-sectional view of the surface of the martensitic steel after annealing at 850 ℃ is shown in Fig. 2. The surface was partly covered with large oxide particles. In other areas the oxide was present as a thin film (Fig. 2.a). The thick layer with a dark contrast is a protective Au coating layer used during the FIB sample preparation. Fig. 2.b. shows the microstructure of the larger surface oxide particles in zone A in Fig. 2.a. These lens-shape oxides particles on the surface had a thickness in the range of 35-130 nm. They were covered by the shell with a different composition. Fig. 2.c. is the lattice image of the interface between the lens-shaped particles and the thin surface film (zone a_1 in Fig. 2.b). The larger particles had an amorphous core and a crystalline shell, which were identified as *a*-SiO_2 and *c*-x$MnO.SiO_2$ ($1 \leq x < 2$), respectively. The black dotted line in Fig. 2.c indicates the position of the interface between the crystalline *c*-x$MnO.SiO_2$ ($1 \leq x < 2$) shell and the amorphous *a*-SiO_2 core. The white dotted line indicates the position of the interface between the shell and the steel matrix. Fig. 2.d is a lattice image taken in zone a_2 of Fig. 2.b.

There is a clear transition layer with a gray contrast in the TEM micrograph visible between the amorphous *a*-SiO_2 core and the crystalline *c*-x$MnO.SiO_2$ ($1 \leq x < 2$) shell, in which the ratio x of Mn to Si increased, corresponding to the transition from amorphous *a*-SiO_2 to crystalline *c*-x$MnO.SiO_2$ ($1 \leq x < 2$). Fig. 2.e is a detail of the surface smaller particles and the thin oxide film with a thickness of ~15 nm. The lattice image of the smaller oxides in zone a_3 of Fig. 2.e is shown in Fig. 2.f. It is amorphous *a*-xMnO.SiO2 with a ratio of Mn to Si less than 0.9. The dotted white line indicates the position of the interface between the amorphous *a*-x$MnO.SiO_2$ ($x < 0.9$) oxide and the steel matrix. The lattice image of the thin oxide film (Fig. 2.g) in zone a_4 of Fig. 2.e was identified as crystalline *c*-x$MnO.SiO_2$, with a Mn/Si ratio larger than 1. The position of the interface between the oxide film and the matrix is indicated by the white dotted line. The

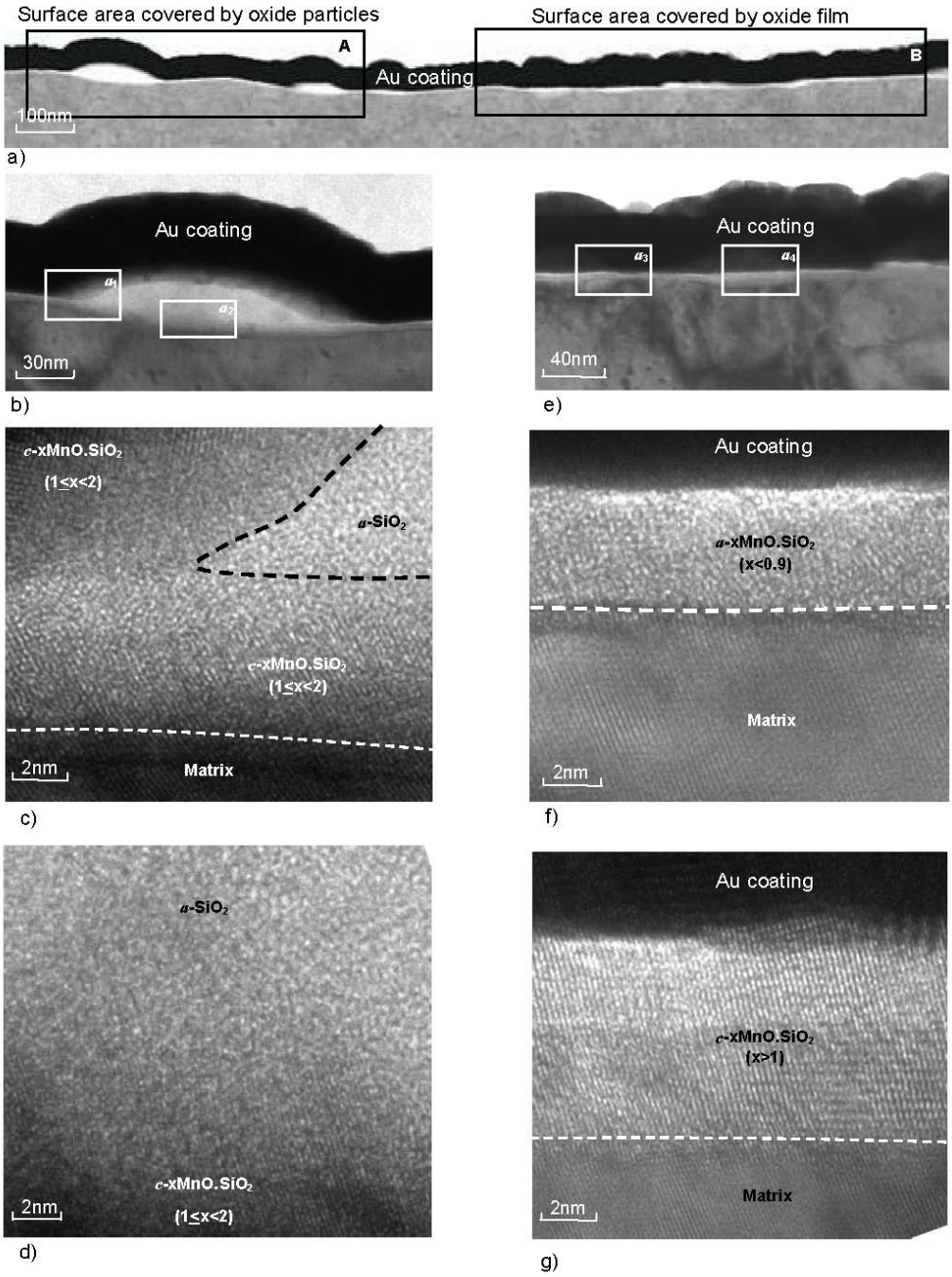

Fig. 2. Cross-sectional TEM micrographs for martensitic steel after annealing prior to hot dipping. (a) Overview of the surface after annealing at 850 ℃, a temperature in the full austenite phase temperature range. At the surface, large oxide particles (zone A) and a thin oxide film (zone B) are clearly visible. (b) Micrograph of the larger oxide particle in zone A. (c) Lattice image of the interface between oxide particles, oxide film and matrix in zone a_1 of (b). The dotted black line indicates the position of the interface between the core of an amorphous a-SiO_2 oxide and its crystalline c-xMnO.SiO_2 ($1 \leq x<2$) shell. The dotted white line indicates the position of the steel/c-xMnO.SiO_2 ($1 \leq x<2$) interface. (d) The transition from the amorphous a-SiO_2 oxides core to the crystalline c-xMnO.SiO_2 ($1 \leq x<2$) shell in zone a_2 in (b). (e) Detailed micrograph of the thin oxide film in zone B of (a). (f) Lattice image of the thin amorphous a-xMnO.SiO_2 ($x<0.9$) oxide in zone a_3 of (c). The dotted white line indicates the position of the steel/a-xMnO.SiO_2 ($x<0.9$) interface. (g) Lattice image of the thin oxide film in zone a_4 in (c). The dotted white line indicates the position of the steel/c-xMnO.SiO_2 ($x>1$) oxide film.

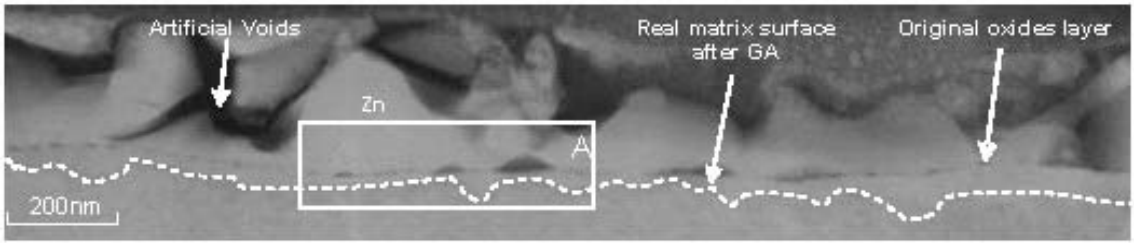

Fig. 3. Cross-sectional TEM micrograph of the steel/coating interface after hot dipping in Zn-0.13Al%. The dotted white line indicates the position of the steel/Zn interface. The string of isolated lens-shaped particles clearly indicates the initial position of the steel surface prior to dipping. The initial crystalline oxide film was clearly removed by a reactive interaction between these surface oxides and the liquid Zn. Zn can therefore penetrate the oxide film and directly react with the steel matrix. Note that the "artificial" voids in the micrographs are solely due to specimen preparation, as most of the Zn layer must be removed prior to FIB sample preparation.

present observations confirm similar observations reported previously by Mahieu *et al.*[2] and Ramadeva *et al.*[9]

Fig. 3 shows the Zn/steel interface after hot dipping in Zn-0.13%Al at 460 ℃. The continuous crystalline oxide films observed after the annealing were almost fully removed after GA. However, the larger amorphous *a*-SiO_2 oxides particles and smaller amorphous particles were still present embedded in the Zn coating. A dotted white line indicates the original position of the steel surface after GA. It is clear that the liquid Zn penetrated through the oxide film and surrounded the amorphous particles. The depth of the former surface "etched" away by the liquid Zn during the dipping process was approximately 60nm.

A detailed microstructure of zone A in Fig. 3 is shown in the micrographs shown in Fig. 4. Fig. 4.a. gives an overview of the oxides layers on the steel surface. Fig. 4.b is a lattice image of the original crystalline film (zone a_1 of Fig. 4.a) after hot dipping. Most of this layer was dissolved due to reduction by the Al in the Zn-0.13%Al bath. The particle with the light contrast was $xMnO.Al_2O_3$ (x=0.8). It is the product resulting from the reduction of the crystalline *c*-$xMnO.SiO_2$ (x>1) by Al. The dotted white line in Fig. 4.c indicates the position of the interface between the matrix and Zn layer, in the area corresponding to zone a_2 in Fig. 4.a. After the crystalline oxides were reduced by Al, they very likely dissolved in the liquid Zn as they were not detected after hot dipping. The Zn penetrated through the oxide film and, as the Fe dissolved in the liquid Zn, the Zn could flow around the larger amorphous oxide particles.

A lattice image of an amorphous *a*-$xMnO.SiO_2$ (x<0.9) particle, corresponding to the zone a_3 of Fig. 4.a, is shown in Fig. 4.d. Amorphous particles with a light contrast are believed to be partially reduced amorphous *a*-$xMnO.SiO_2$ (x<0.9). The product of the reduction reaction, $xMnO.Al_2O_3$ (x=0.6), was found close to these amorphous *a*-$xMnO.SiO_2$ (x=0.3) oxides. Fig. 4.e shows a detailed microstructure of what was originally an amorphous *a*-SiO_2 particle with a crystalline *c*-$xMnO.SiO_2$ ($1 \leq x < 2$) shell, corresponding zone a_4 of Fig. 4.a. The light contrast phase forming around the amorphous *a*-SiO_2 particle is $xMnO.Al_2O_3$ ($0.2 < x < 1.25$) after the hot dipping, as the original crystalline *c*-$xMnO.SiO_2$ ($1 \leq x < 2$) shell was reduced by Al. The amorphous *a*-SiO_2, corresponding to zone a_5 of Fig. 4.a, is shown in Fig. 4.f. The lattice image of amorphous *a*-SiO_2 clearly shows that this particular oxide was not reduced by Al during dipping.

The microstructure of the coating/steel interface after hot dipping in Zn-0.20%Al at 460 ℃ is shown in Fig. 5. The thick layer with a darker gray contrast in Fig. 4.a is the inhibition layer. Its thickness was irregular. The original steel surface was "etched" by the liquid Zn, and the residual oxides were found to be entirely embedded in the inhibition layer (Fig. 5.a). Fig. 5.b shows a lattice image of the inhibition layer, corresponding to zone A in Fig. 5.a. The composition of the inhibition layer was $Fe_2Al_{5-x}Zn_x$ ($0.12 < x < 0.6$). The dotted white line in Fig. 5.c indicates the position of the interface between the inhibition layer and the matrix. The detailed microstructure of zone B in Fig. 5.a is shown in Fig. 6. The particles with the white contrast in Fig. 6.a are the initial oxides that can still be observed after hot dipping in Zn-0.20%Al. The dotted lines indicate the steel/coating interface position after hot dipping. Fig. 6.b shows the microstructure for amorphous *a*-SiO_2 particles, which had a *c*-$xMnO.SiO_2$ ($1 \leq x < 2$) oxide shell prior to hot dipping (e.g. in zone a_1 of Fig. 1.a). The amorphous *a*-SiO_2 particles were still present after dipping, but the *c*-$xMnO.SiO_2$ ($1 \leq x < 2$) oxide shell was reduced to $xMnO.Al_2O_3$ ($0.8 < x < 2.8$). The reduction is very likely by the Al present in the Zn-0.20Al% bath. Fig. 6.c shows some residue of the initial oxides film (zone a_2 in Fig. 6.a). The dotted white lines indicate

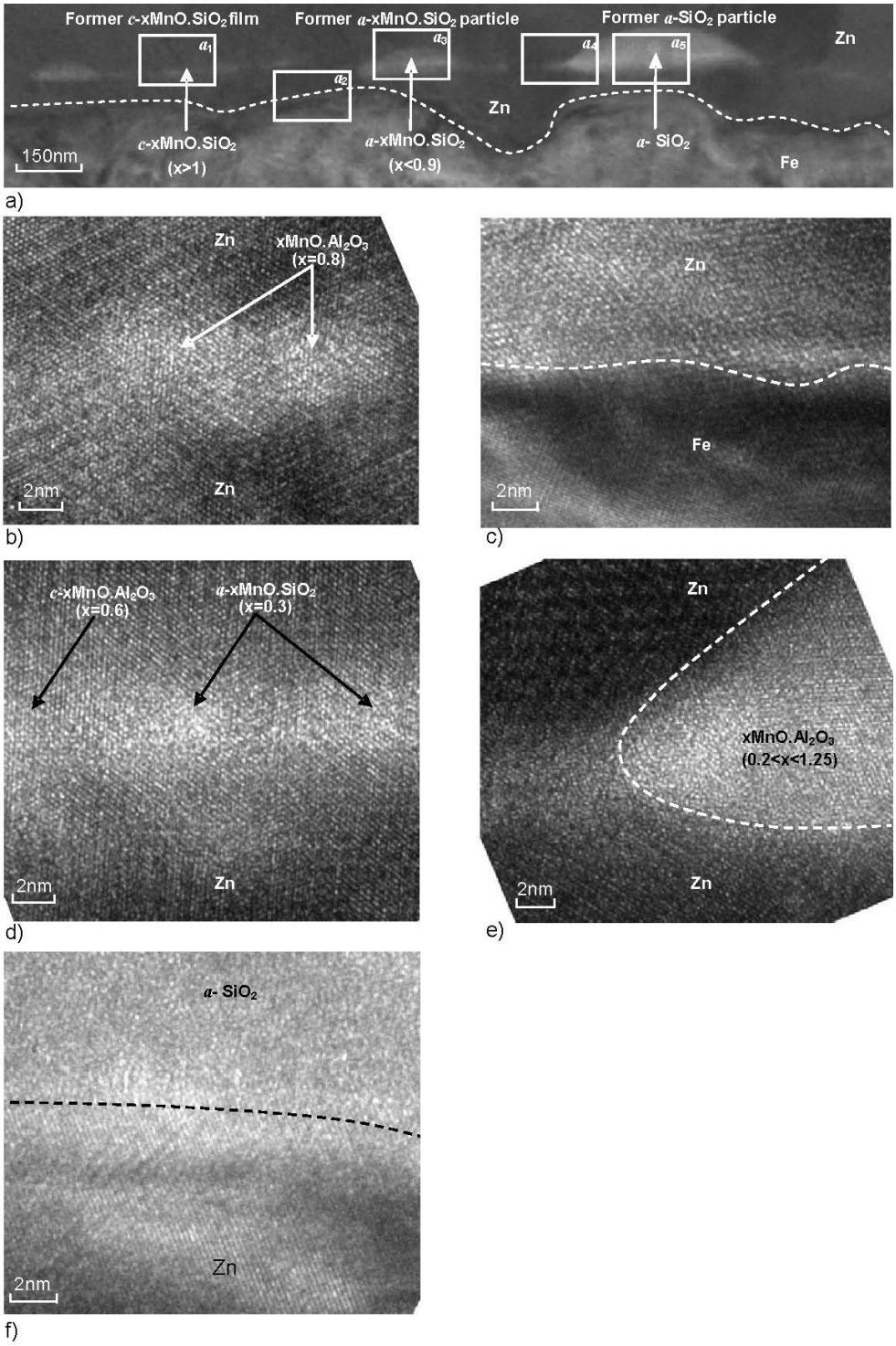

Fig. 4. (a) Cross-sectional TEM micrograph of the martensitic steel/coating interface after hot dipping in Zn-0.13%Al. The white dotted line indicates the steel/coating interface. Note the absence of the $Fe_2Al_{5-x}Zn_x$ inhibition layer. (b) Lattice image for *c*-xMnO.Al_2O_3 (x=0.8) formed by reduction of the *c*-xMnO.SiO_2 (x>1) oxide by Al. (c) Lattice image of the steel/Zn interface. The Zn has penetrated through the crystalline oxides after their reduction by Al. (d) Lattice image of small residual *a*-xMnO.SiO_2 (x<0.9) oxide particles of the zone a_3 in (a). The *a*-xMnO.SiO_2 (x<0.9) oxides cannot be completely reduced by Al. (e) Lattice image of the *c*-xMnO.Al_2O_3 oxide shell around an amorphous *a*-SiO_2 particles. (f) Lattice image of an *a*-SiO_2 oxide particle embedded in the Zn.

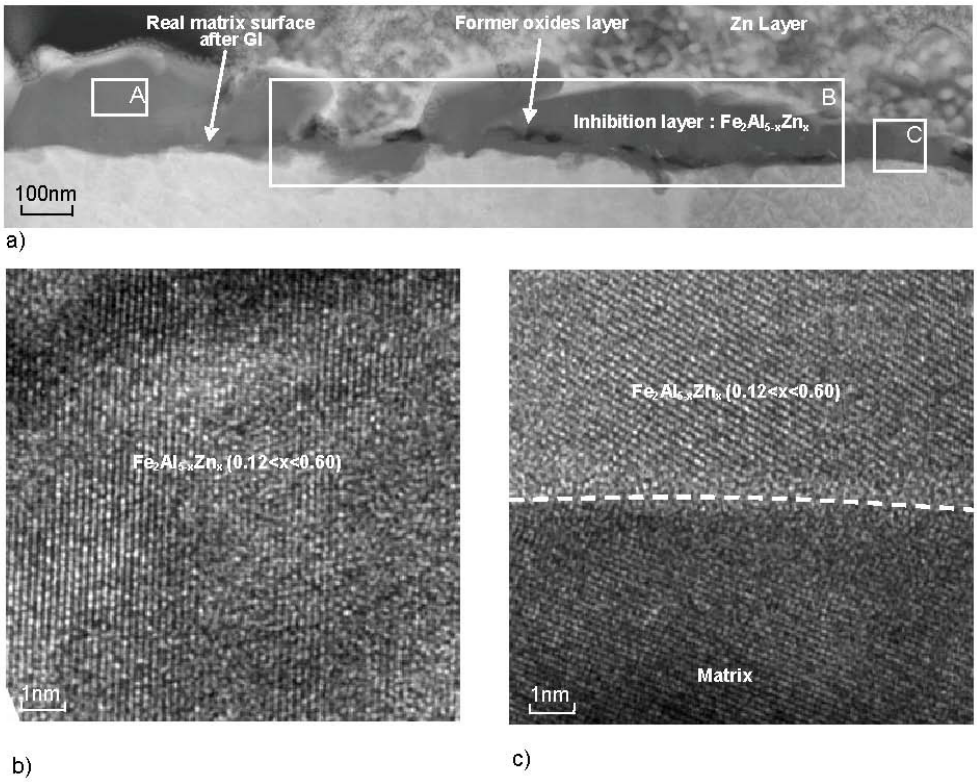

Fig. 5. Cross-sectional TEM micrographs of the steel/inhibition layer interface after hot dipping of the martensitic steel in Zn-0.2%Al. (a) Overview of the inhibition layer with embedded residual oxides. (b) Lattice image of the $Fe_2Al_{5-x}Zn_x$ inhibition layer in zone A in (a). (c) Steel/$Fe_2Al_{5-x}Zn_x$ interface in zone C of (a).

the position of the initial crystalline oxide film, which was almost completely removed during the hot dipping. The Zn coating side of the $Fe_2Al_{5-x}Zn_x$ inhibition layer had a value for x in the range of 0.44-0.60. The matrix-side of the inhibition layer was less enriched in Zn rich. Its x value was in the range of 0.14-0.32. Fig. 6.d shows a detailed microstructure of an initially thicker crystalline oxide layer (zone a_3 in Fig. 6.a). These thicker crystalline *c*-$xMnO.SiO_2$ (x=1.41) oxides initially present on the surface prior to the hot dipping were not completely reduced due to their thickness and they could therefore still be observed embedded in the inhibition layer after hot dipping. The product of the reduction reaction, $xMnO.Al_2O_3$ ($0.8<x<2.8$), is also shown in Fig. 6.d.

Van De Putte *et al*. recently used sessile drop angle measurements to analyze the effects of Si-Mn oxides on the wettability of the Si-bearing steel sheets by analysis of the wetting angel.[14] Khondker *et al*. and Bellouse *et al*. have suggested that MnO oxides can be reduced by Al during hot dipping,[11),12)] according to the following reaction:

$$3MnO + 2Al_{sol} \Rightarrow Al_2O_3 + 3Mn_{sol}$$

However, the reactive interaction between Al in the liquid Zn and the $xMnO.SiO_2$ compound oxides was not considered. An alternative two-step reduction process occurring during hot dipping could be as follows:

$$Mn_2SiO_4 + 2Al_{sol} \Rightarrow [MnO]MnSiO_3 + 2Al_{sol}$$
$$Mn_2SiO_4 + 2Al_{sol} \Rightarrow [Al_2O_3] + Mn_{sol} + Si_{sol}$$
$$\overline{Mn_2SiO_4 + 2Al_{sol} \Rightarrow [MnAl_2O_3] + Mn_{sol} + Si_{sol}}$$

Note that this formal reaction mechanism takes into account two compound oxides $MnO.SiO_2$ and $2MnO.SiO_2$. The first reaction is strictly speaking not a reduction reaction, but it emphasizes the fact that the reduction of $2MnO.SiO_2$ goes via the intermediate formation of $MnSiO_3$. In addition, the proposed reactions underline the importance of the very high thermodynamic stability of the $MnAl_2O_4$ spinel in driving the reduction reactions. It also suggests how the oxides can appear to dissolve into the liquid Zn, leaving $MnAl_2O_4$ as a reaction product.

The mechanical properties of hot dipped martensitic steels were evaluated by means of uni-axial tensile tests. Engineering stress-strain curves for the as-quenched and galvanized specimens are shown in Fig. 7. The stress-

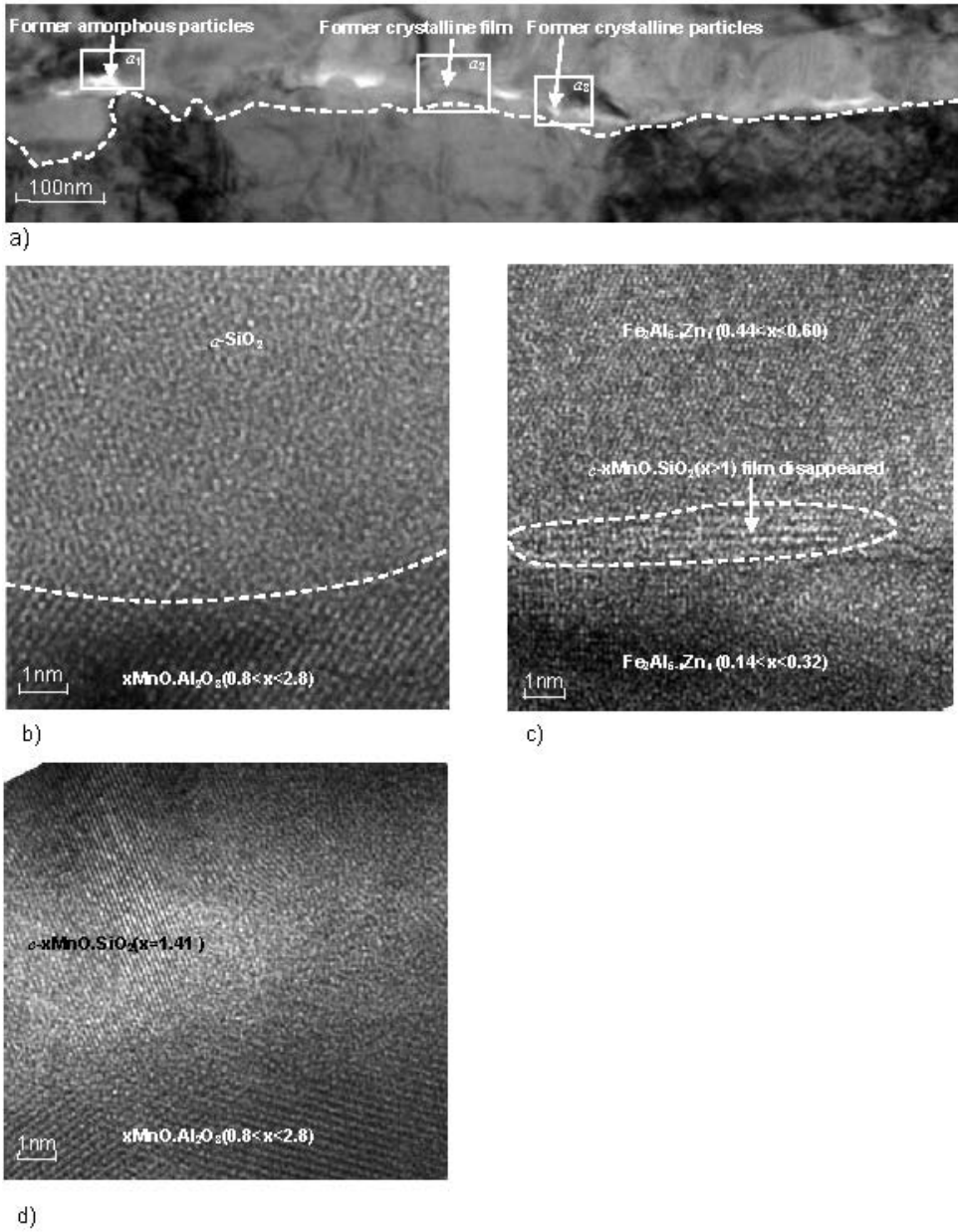

Fig. 6. (a) Cross-sectional TEM image of zone B in Fig. 5.a, showing oxides particles embedded in the inhibition layer. The dotted white line indicates the position of the steel/inhibition layer after dipping. Particles with a light contrast are the initial oxides particles. (b) Lattice image of the amorphous oxide particles of zone a_1 in a. The amorphous a-xMnO.SiO_2 (x<0.9) and a-SiO_2 particles were not reduced by Al. (c) Lattice image of a residue of the crystalline c-xMnO.SiO_2 (x>1) oxide film in zone a_2 of (a). (d) Lattice image of a small crystalline xMnO.SiO_2 (x>1) particle partially reduced by Al. The particle is surrounded by c-xMnO.Al_2O_3 (0.8<x<2.8) oxide, which is the product oxide of the Al reduction.

strain curve of the as-quenched martensite shows the characteristic continuous stress-strain curve for low-carbon lath martensite. Its ultimate tensile strength (UTS) and total elongation were 1460 MPa and 5.8%, respectively. The hot dip process resulted in a significant decrease of the UTS by about 300 MPa. The total elongation increased to 12%. The difference in mechanical properties between as-quenched and galvanized specimen was due to the presence bainite. During the slow cooling from 480 ℃ to the dipping temperature of 460 ℃, part of the untransformed austenite inevitably transformed to bainite. The presence of bainite in the martensite matrix reduced the strength of the steel, and improved the ductility. This implies that the strength and elongation of martensitic steel can be con-

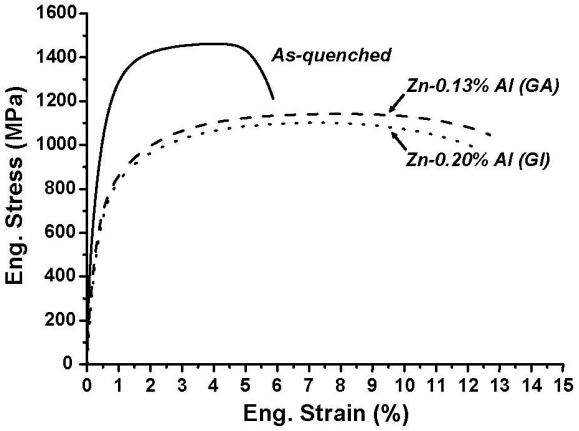

Fig. 7. Engineering stress-strain curves for water quenched martensite and galvanized materials.

trolled by adjusting the process parameters within the process window available in a conventional hot dip galvanizing processing line.

4. Conclusions

The selective oxidation of Si and Mn on the surface of a martensitic steel annealed in a 10%H_2 + N_2 gas atmosphere in conditions of external oxidation, i.e. with a dew point of -35 ℃, resulted in the formation of amorphous *a*-SiO_2 particles with a crystalline xMnO.SiO_2 (1 x<2) oxide shell, small amorphous a-xMnO.SiO_2 (x<0.9) particles and a very thin crystalline c-xMnO.SiO_2 (x>1) film at the steel surface.

During hot dipping in Zn-0.13%Al, the thin c-xMnO.SiO_2 (x>1) crystalline oxide film was reduced by Al and dissolved in the liquid Zn. The crystalline xMnO.SiO_2 (1 x<2) oxides shell of amorphous *a*-SiO_2 particles was reduced to xMnO.Al_2O_3 (0.2<x<1.25). The amorphous *a*-xMnO.SiO_2 (x<0.9) and *a*-SiO_2 particles were not reduced during hot dipping and remained embedded in the Zn layer. No inhibition layer was formed during dipping in Zn-0.13%Al.

After hot dipping in Zn-0.20%Al, the thin c-xMnO.SiO_2 (x>1) crystalline oxide film was reduced by Al and dissolved in the liquid Zn. The crystalline c-xMnO.SiO_2 (1 x<2) oxides shell of amorphous *a*-SiO_2 particles was reduced to xMnO.Al_2O_3 (0.8<x<2.8). Amorphous *a*-xMnO.SiO_2 (x<0.9) and *a*-SiO_2 particles were not reduced and were imbedded in the $Fe_2Al_{5-x}Zn_x$ inhibition layer.

The observed results clearly show that Al in the Zn bath plays a critical role in reducing the crystalline *c*-xMn.SiO_2(x>1) compound oxides formed at the surface of a martensitic steel during austenitic annealing. The amorphous *a*-xMnO.SiO_2 (x<0.9) and *a*-SiO_2 oxides particles were essentially unaffected by the hot dipping.

References

1. A. R. Marder, *Progr. Mater. Sci.*, **45**, 193 (2000).
2. J. Mahieu, S. Claessens, and B. C. De Cooman, *Metall. Mater. Trans. A*, **32A**, 2905 (2001).
3. X. Vanden Eynde, J. P. Servais, and M. Lamberigts, *Surf. Interface Anal.*, **35**, 1004 (2003).
4. Y. F. Gong, S. Birosca, Han S. Kim, and B. C. De Cooman, *J. Microsc.*, **230**, 424 (2008).
5. J. Mahieu, S. Claessens, B. C. De Cooman, and F. Goodwin, Proceedings of the 6th International Conference on Zinc and Zinc Alloy Coated Steel Sheet (Galvatech), p. 529, M. A. Baker Editor, Association for Iron and Steel Technology, Chicago, Illinois (2004).
6. Y. F. Gong, Han S. Kim, and B. C. De Cooman, *ISIJ International*, **49**, 557 (2009).
7. Y. F. Gong, Han S. Kim, and B. C. De Cooman, *ISIJ International*, **48**, 1745 (2008).
8. Xiang Shu Li, Sung-Il Baek, Chang-Seok Oh, Sung-Joon Kim, and Young-Woon Kim, *Scripta Mater.*, **57**, 113 (2007).
9. C. Ramadeva Shastry, John A. Rotole and Thomas W. Kaiser, Proceedings of the 7th International Conference on Zinc and Zinc Alloy Coated Steel Sheet (Galvatech), p. 403, Association for Iron and Steel Technology, Osaka, Japan (2007).
10. D. Huin, P. Flauder, and J. B. Leblond, *Oxidation of Metals*, **64**, 132 (2005).
11. R. Khondker, A.I. Mertens, and J. R. McDermid, *Mater. Sci. Eng. A*, **463**, 157 (2007).
12. E. M. Bellouse, A.I. Mertens, and J.R. McDermid, *Mater. Sci. Eng. A*, **463**, 147 (2007).
13. R. J. Meguerian and J. R. McDermid, Materials Science and Technology 2007 Conference and Exhibition (MS& T'07), p. 569, the Minerals, Metals & Materials Society (TMS), Detroit, USA (2007).
14. T. Van De Putte, D. Loison, J. Penning, and S. Claessens, *Metall. Mater. Trans. A*, **39A**, 2875 (2009).
15. J. Mahieu, Doctoral Thesis, p. 79, Ghent University, Ghent, Belgium (2006).